Journal of
Marine Science and Engineering

MDPI

Article

Research on Effect of Ship Speed on Unsteady Hydrodynamic Performance of Bow Thrusters in Berthing and Departure Directions

He Cai [1], Xiaoqian Ma [1], Tan Wen [1], Yu Sun [2,*], Zhiyuan Yang [3], Yilong Tan [3] and Jianyu Zhuo [4]

[1] Shanghai Marine Equipment Research Institute, Shanghai 200031, China; he_cai@sina.com (H.C.); ryemond@sina.com (X.M.); wentan0316@163.com (T.W.)
[2] College of Ocean Science and Engineering, Shanghai Maritime University, Shanghai 201306, China
[3] Merchant Marine College, Shanghai Maritime University, Shanghai 201306, China; yangzy@shmtu.edu.cn (Z.Y.); 202330110110@stu.shmtu.edu.cn (Y.T.)
[4] China Classification Society, Beijing 100007, China; jyzhuo@ccs.org.cn
* Correspondence: sunyu@shmtu.edu.cn

Abstract: With the continuous development of the shipping market, bow thrusters have become more important for ship maneuvering. Therefore, the performance of bow thrusters is studied in this paper. In order to obtain an unsteady performance of the bow thruster under different ship speed conditions, the SST k-ω turbulence model is adopted to predict the hydrodynamics of the bow thruster. With the ship's speed increasing gradually, the variation characteristics of hydrodynamic coefficients and the flow field distribution at key positions are analyzed. The results show that with an increase in ship speed to three knots, the thrust coefficient and torque coefficient of the bow thruster decrease by 2.69~4.07% and 2.34~3.08%. In addition, the blade vibration amplitude intensifies. In the departure direction, the propeller load is more susceptible to being influenced and decreases by an additional 2.34~4.16% compared with that in the berthing direction. Meanwhile, it is found that the velocity distribution is asymmetrical. The inlet velocity at the bow side is faster, which results in the maximum peak pressure being about three times the minimum peak pressure. In addition, the pressure's nonuniformity in the tunnel increases gradually with the increase in ship speed. Compared with the pressure distribution in the berthing direction, the pressure distribution before and after the propeller is more uniform, which is consistent with the results of hydrodynamic change and velocity distribution. The research in this paper has a certain reference significance for understanding the hydrodynamic performance of bow thrust operation.

Keywords: bow thruster; hydrodynamic performance; numerical simulation; SST k-ω turbulence model

Citation: Cai, H.; Ma, X.; Wen, T.; Sun, Y.; Yang, Z.; Tan, Y.; Zhuo, J. Research on Effect of Ship Speed on Unsteady Hydrodynamic Performance of Bow Thrusters in Berthing and Departure Directions. *J. Mar. Sci. Eng.* **2024**, *12*, 2054. https://doi.org/10.3390/jmse12112054

Academic Editor: Decheng Wan

Received: 13 August 2024
Revised: 4 October 2024
Accepted: 6 October 2024
Published: 13 November 2024

1. Introduction

Due to improvements in the positioning and maneuverability requirements of ships, bow thrusters have become an indispensable auxiliary propulsion device on ships. Their original intention was to improve the flexibility and accuracy of the ship in the maneuvering process so that the ship has good maneuvering performance under special conditions such as berthing, leaving, or emergency refuge and sailing in narrow waters. Hydrodynamic performance is the most basic performance of bow thrusters, and there is also an abundance of research on bow thrusters.

At present, plenty of experimental research and numerical simulations on bow thrusters have been carried out. Fischer [1] studied the high noise and vibration caused by bow thrusters and high underwater radiation noise and proposed a method to reduce noise and vibration. Herdzik [2] pointed out that different from traditional propulsions, bow thrusters could improve the propulsion efficiency of ships and completely change their maneuverability pattern. Wilkins [3] carried out an optimization design of the tunnel

bow propeller under the tension of the mooring column, and most studies evaluated the efficiency of a single bow thruster installation. Yao and Yan [4] observed the effects of the pitch ratio, extended area ratio, boss ratio, and tunnel length on the performance of bow thrusters without ship speed. The results showed that tunnel length has a great influence on efficiency. Terry [5] explored the interaction of two bow thrusters and found that there were strong interactions among multiple thrusters. Wang et al. [6] studied the characteristics of bow thrusters. The simulation results proved the correctness of the model, which can provide theoretical support for large ships. Theophilus-Johnson [7] analyzed the design of fast bow thrusters and found that their performance efficiency was proportional to the thrust provided, and the thrust and torque generated were inversely proportional to the diameter of the propeller. Feng et al. [8] conducted an in-depth study on the hydrodynamic performance of bow thrusters through experimental and numerical simulation methods. It was found that the hull, the inlet angle, and the guide hood on the hull had important effects on the performance of bow thrusters. Teresa [9] conducted an experimental study on the performance of bow thrusters in terms of the flow field generated and the hydrodynamic force generated on the hull. Then, the multi-objective optimization [10] of bow thrusters was based on numerical simulation to improve their propulsion efficiency by changing the chamfer form of the bow thruster tunnel opening and the position of the back suction tunnel. Bui [11] used the RANS method to simulate the hydrodynamic characteristics of bow thrusters. The results showed that the thrust coefficient results of the SST k-ω turbulence model are more accurate. Huang et al. [12] used the RANS method to study the hydrodynamic performance of tunnel thrusters under berthing and berthing conditions. M. Kazemi et al. [13] conducted scale decomposition simulations of unsteady bow thruster hydrodynamics. The results indicated that the differences between the turbulence models were negligible.

In addition, many investigations into the hydrodynamic performance of ship propulsions also have reference value to this paper. Li [14] numerically calculated the open water characteristics of a highly skewed propeller under a full-scale propulsion condition. It was found that the grid density had little effect on the prediction of open water characteristics. Song et al. [15] studied the open water performance difference between the hub-type Rim-Driven Thruster (RDT) and hubless RDT by CFD analysis, and the simulation results showed that the efficiency of the hubless RDT was higher than that of the hubless RDT. Tu [16] used the RANS method with the sliding mesh method to simulate the open water characteristics of the propeller. It was found that under the same grid type, the calculation result of the SST k-ω turbulence model was slightly better. Guo et al. [17] studied the hydrodynamic characteristics of the propeller in the oblique inflow using the CFD method. The effect of lateral inflow on the hydrodynamic characteristics of the propeller was proven. Lee et al. [18] modified the propeller blade by the serrated structure, and the noise reduction effects of three different serrated shapes were compared. Huang et al. [19] predicted the hydrodynamics and flow noise of the pump-jet propulsor without tip clearance. After comparison, it was found that tip vortex control played a role in vibration and noise reduction. Qin et al. [20] and Sun et al. [21,22] adopted a serrated trailing edge for the spanwise correlation reduction in the propulsion duct wake. The results showed that under the same conditions, the serrated trailing edge significantly reduced the wake vortex intensity and produced a certain noise reduction effect in the radial direction.

From the research progress on the hydrodynamic performance of bow thrusters, it can be seen that most scholars are concerned with the hydrodynamic performance of bow thrusters in calm water under mooring conditions, which is an ideal environment. However, during departure and berthing, a ship may navigate at low speeds, so it is necessary to analyze the impact of the ship's speed on the bow thruster. In addition, there are many studies on the hydrodynamic characteristics of propellers, which provide rich reference cases for the numerical analysis in this paper and allow us to improve our own simulation models.

In this paper, the hydrodynamic performance of bow thrusters is studied by numerical simulation. The SST k-ω turbulence model is used to predict the hydrodynamic performance of bow thrusters under different operation conditions. According to the variation characteristics of hydrodynamic coefficients and the flow field distributions at key positions, we summarize the impact of ship speed on bow thruster performance.

2. Theories and Formulas

2.1. Flow Model

The flow simulation of this paper is carried out by using the solution technique implemented in Fluent 2022 R1. The details are introduced below.

Assuming that the fluid is incompressible, the continuity equation and momentum equation [23] of the flow field are, respectively,

$$\frac{\partial u_i}{\partial x_i} = 0 \tag{1}$$

$$\frac{\partial(\rho u_i)}{\partial t} + \nabla(\rho u_i \boldsymbol{u}) = \nabla(\mu \nabla u_i) - \frac{\partial p}{\partial x_i} + S_i \tag{2}$$

where u_i is the mean value of velocity component (i = 1, 2, 3); p is the time mean of pressure; ρ and μ are the fluid density and viscosity coefficient, respectively; t is time; S_i is a generalized source term.

The turbulence model adopted in this paper is the SST k-ω model, which is a shear stress transport model proposed by Menter [24] and also introduced by Tu et al. [25]. The default wall function of the SST k-ω model is adopted in this paper. The solution method is a pressure-based solver, and the SIMPLEC algorithm is used in pressure–velocity coupling. The gradient term is selected as one that is Least Squares Cell-Based, and the pressure term is selected as Second Order in the discrete mode. The momentum flux term, turbulent kinetic energy term, and turbulent dissipation rate term are selected as being Second-Order Upwind. The transient formulation is selected as being Second-Order Implicit. The time step is set to the time of two degrees of propeller rotation, and each time step is iterated 20 times. In the calculation process, the force change in the propeller blade with time is recorded, and the iteration is stopped when the calculation converges. After 1080 time steps (6 rotation cycles), the calculation completely converged. The continuity residuals vary from 3×10^2 to 8×10^4, which drops by two orders of magnitude within a time step. All the hydrodynamic variables mentioned in this paper are regularly periodic changes.

2.2. Dimensionless Hydrodynamic Coefficient of Propeller

After calculation convergence, the hydrodynamic forces of bow thrusters are obtained. The thrust and torque are converted into dimensionless hydrodynamic coefficients [21,22] according to Equation (3).

$$\begin{aligned} \text{Advance coefficient}: \ J &= \frac{V}{nD} \\ \text{Thrust coefficient}: K_{\mathrm{T}} &= T/\rho n^2 D^4 \\ \text{Torque coefficient}: \ K_{\mathrm{Q}} &= Q/\rho n^2 D^5 \\ \text{Propulsive efficiency}: \ \eta &= \frac{J}{2\pi} \cdot \frac{K_{\mathrm{T}}}{K_{\mathrm{Q}}} \end{aligned} \tag{3}$$

where v and n are the advance speed (m/s) and rotational speed (1/s) of the propeller; D is the propeller diameter (m); T and Q are the thrust (N) and torque (N·m), respectively.

3. Computational Model Establishment

3.1. Research Object

The bow thruster on the original ship is a varying pitch propeller of an icebreaker ship, which can work in both the berthing and departure directions. The bow thruster is installed in the bow tunnel, whose diameter is 2850 mm. The bow thruster is illustrated in Figure 1,

and its major parameters are listed in Table 1. Due to the asymmetric position and structure of the bow thruster within the tunnel, the hydrodynamic performance is analyzed in both directions. In addition, the ship draft is 10.3 m, and the distance between the propeller shaft and hull base is 1.7 m. Therefore, the shaft is 8.6 m from the water surface. The Reynolds number of the propeller in all calculated conditions is about 3×10^7.

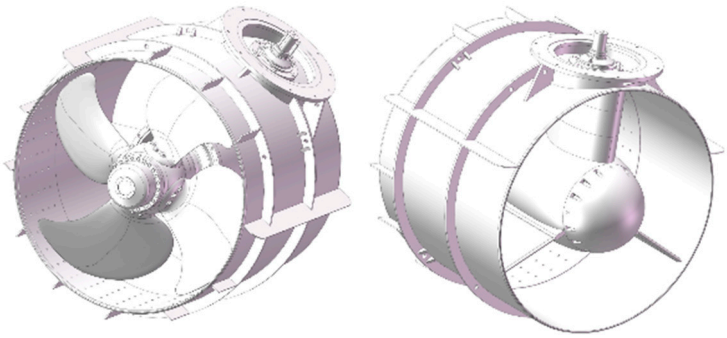

Figure 1. Geometric model of bow thruster.

Table 1. Major parameters of bow thruster.

Parameters	Values
Blade diameter D (mm)	2800
Hub diameter d (mm)	800
Number of blades Z	4
Disk ratio A_E/A_0	0.642

3.2. Geometric Model Processing

In order to carry out the numerical simulation analysis of propeller hydrodynamics, the propeller model is simplified in detail. The simplified propeller model and its position in the tunnel are presented in Figure 2. Since the hull model only includes the bow part below the waterline, the last transverse profile line of the ship's bow model is translated along the direction of ship length as the parallel middle body of the ship, which would not affect the inflow of the propeller. The processed model is shown in Figure 3.

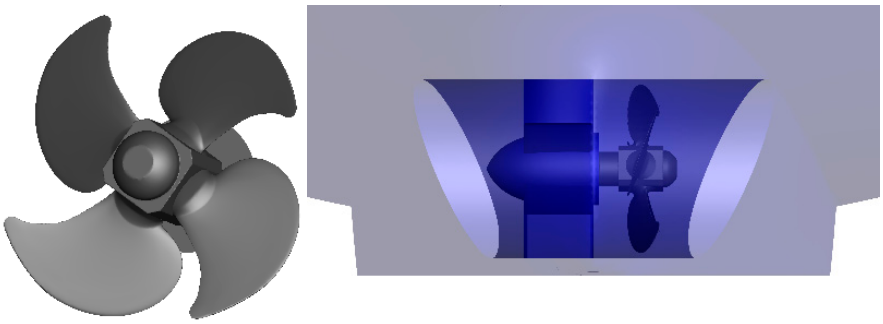

Figure 2. Hydrodynamic model of propeller and its position in tunnel.

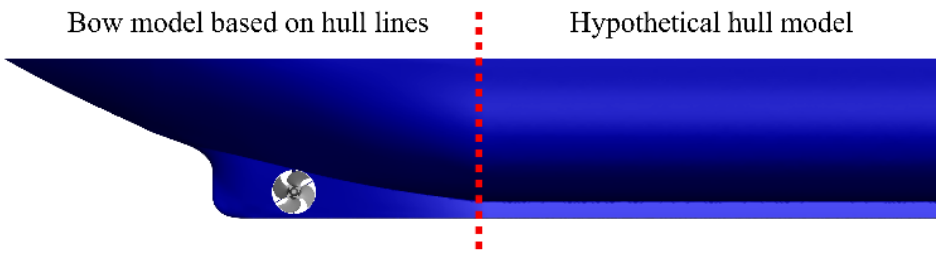

Figure 3. Hydrodynamic model of ship under waterline.

3.3. Computational Domain Establishment

Firstly, the computational domain is built so that the bow thruster can operate in a wide enough water area and its flow field can be fully developed. The sizes and boundary conditions of the established computational domain are illustrated in Figure 4. The inlet turbulence intensity and viscosity ratio are 5% and 10, and they are kept the same in the free stream before the hull region. In order to make the propeller rotate in the tunnel, a cylinder control domain is established. The grids in the control domain are fine, and the surface between the control domain and the external flow field is set as the interface.

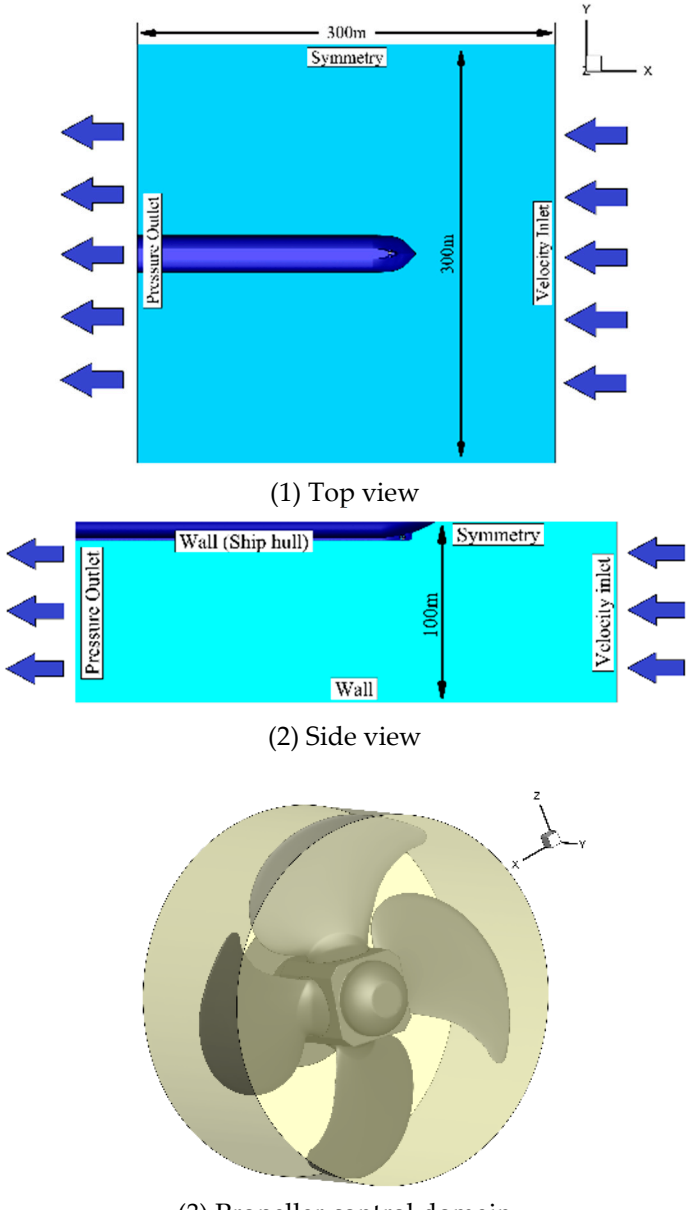

Figure 4. Computational domain and boundary conditions.

3.4. Grid Scheme and Independence Verification

After the computational domain is established, polyhedral grids and boundary layer grids are used to divide the entire flow field, and the grids in the control domain are fine. The boundary layer grids are structured in the wall-normal direction, consisting of 10 layers. The thickness increase ratio is 1.1. The y^+ value is mainly affected by the propeller rotation speed instead of the ship speed. Therefore, the y^+ value of the computational

model is controlled within 150 according to the propeller rotation speed, which is used for all resolutions. The grid scheme is shown in Figure 5.

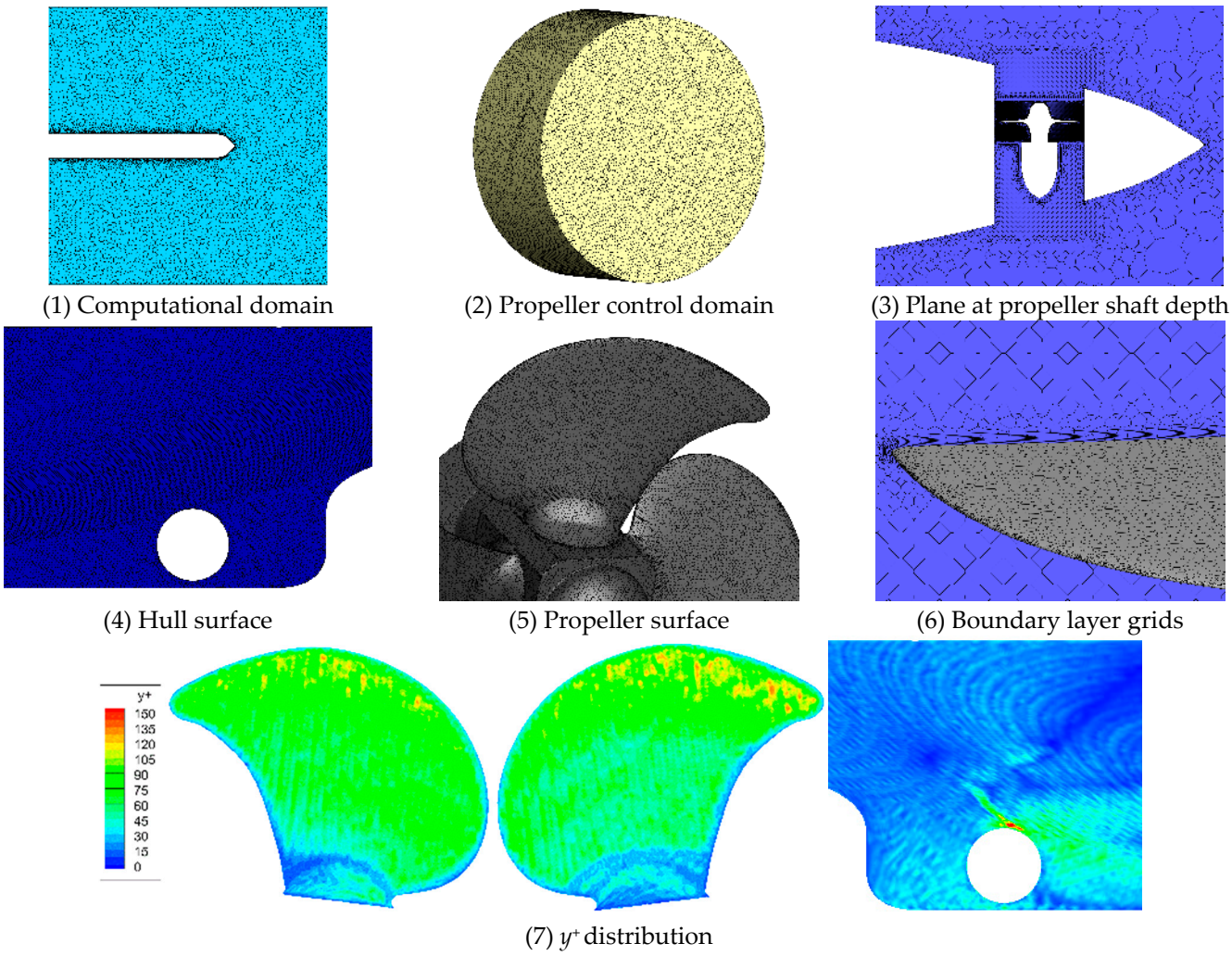

Figure 5. Grid scheme and y^+ value of computational model.

In order to eliminate the influence of grid size on the hydrodynamic prediction accuracy, three grid schemes with different grid densities are named Coarse, Medium, and Fine according to the density, of which the total number of grids is 10.7 million, 15.0 million, and 20.5 million, respectively. When the ship speed is 0 kn and the propeller rotation speed is 243 rpm, the calculation results of the three gird schemes are shown in Table 2. Because the ship did not move laterally, the bow thruster does not perform any work in the lateral direction of the ship, and its efficiency is 0. It can be concluded that the excessive encryption of the grids would not significantly improve calculation accuracy but would reduce computational efficiency. Therefore, the medium grid scheme is used for the hydrodynamic performance prediction of the bow thruster.

Table 2. Hydrodynamic results of three grid schemes.

Grid Scheme	K_T	K_Q
Coarse	0.1731	0.02522
Medium	0.1743	0.02537
Fine	0.1752	0.02545

3.5. Reliability Analysis of Computational Model

Many propeller diagrams and open water tests have been designed for Ka series ducted propellors, which can provide rich hydrodynamic performance data resources. Therefore, the computational model reliability of the bow thruster is verified by the Ka series propeller with a 19A duct. Errors between the simulation results and experimental results are observed. The ducted propeller with its grids is given in Figure 6.

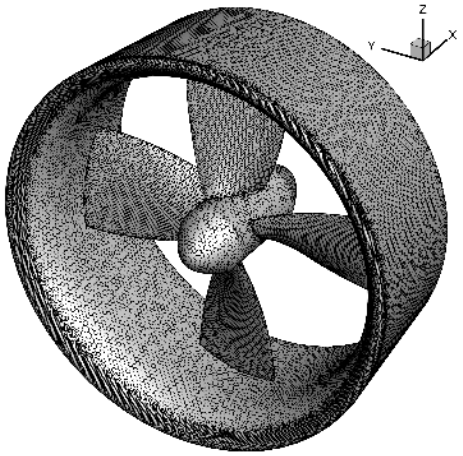

Figure 6. Ducted propeller with its grid scheme.

According to Equation (3), the simulation results of the ducted propeller are converted into thrust coefficient K_T, torque coefficient K_Q, and propulsion efficiency η, and they are compared with the experimental results in the literature [26]. As shown in Figure 7, the errors of K_T, K_Q, and η are all within 3%, which is basically consistent with the results in the literature. Therefore, it is considered that the calculation model established in this paper is suitable for the hydrodynamic analysis of bow thrusters.

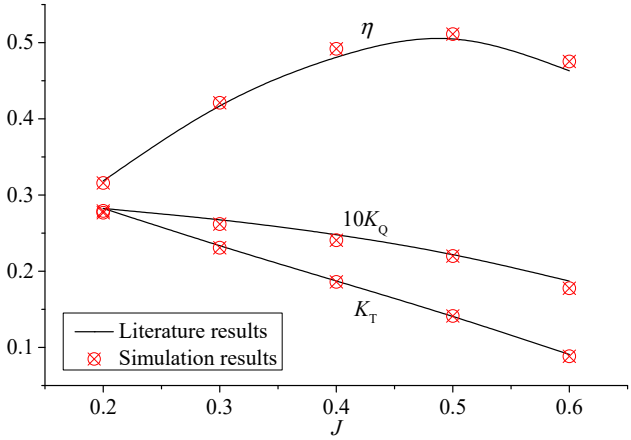

Figure 7. Open water performance curves of ducted propeller.

4. Results and Discussion

After verifying the calculation model in this paper, the hydrodynamic performance of the bow thruster is analyzed, and the results with its analysis are as follows.

4.1. Hydrodynamic Performance Analysis of Bow Thruster

Because of the hull's influence, the pressure distribution of the blades at different phases is constantly changing. When n is 243 rpm and v is 0 knots, the blade pressure distribution is as shown in Figure 8. It can be seen that the pressure distribution of the four blades is significantly different, among which the pressure difference between the suction

side and the pressure side of the lower blade is the largest. Accordingly, the force of this blade is the largest. In contrast, the pressure difference between the two sides of the upper blade is smaller, and the force is the smallest. Therefore, the bow thruster blades have large force fluctuations in a rotation cycle.

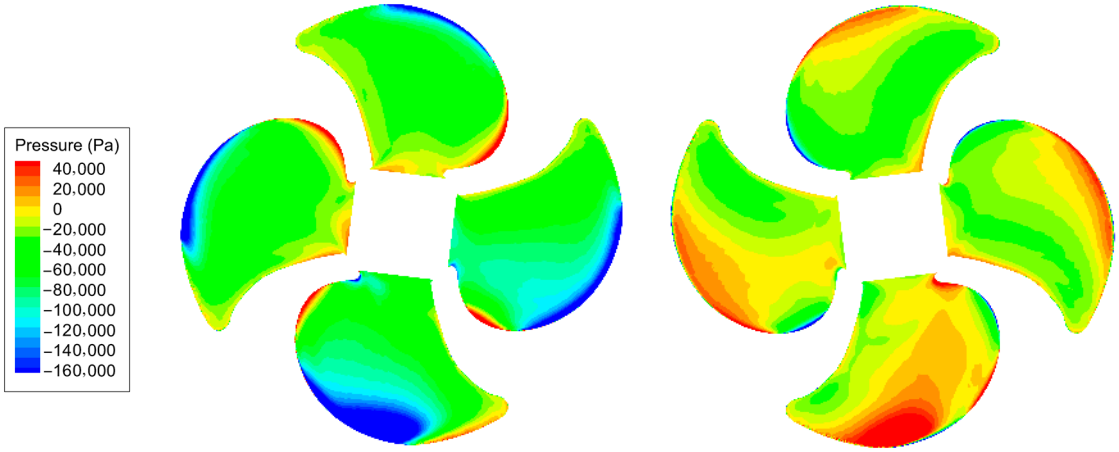

Figure 8. Pressure distribution on the blades (**left**: pressure side, **right**: suction side).

In order to analyze the pressure of the tunnel, the pressure pulsations at the key positions are observed. Twelve monitoring points are uniformly arranged on the propeller disk. The locations of the monitoring points and their peak pressures are shown in Figure 9, and the pressure pulsations are illustrated in Figure 10.

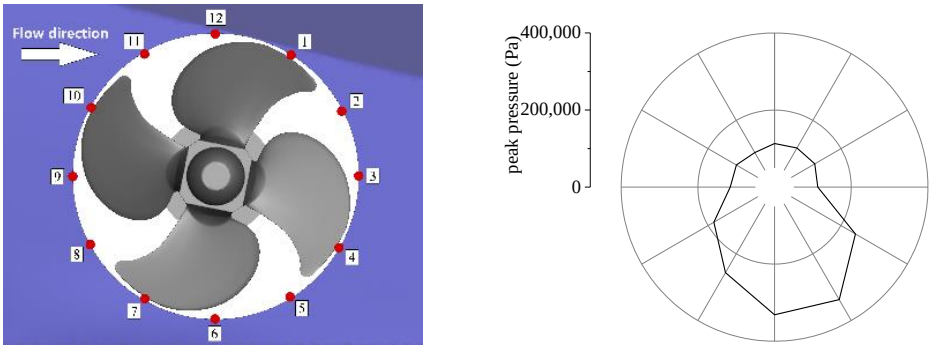

Figure 9. Monitoring point positions with their peak pressures.

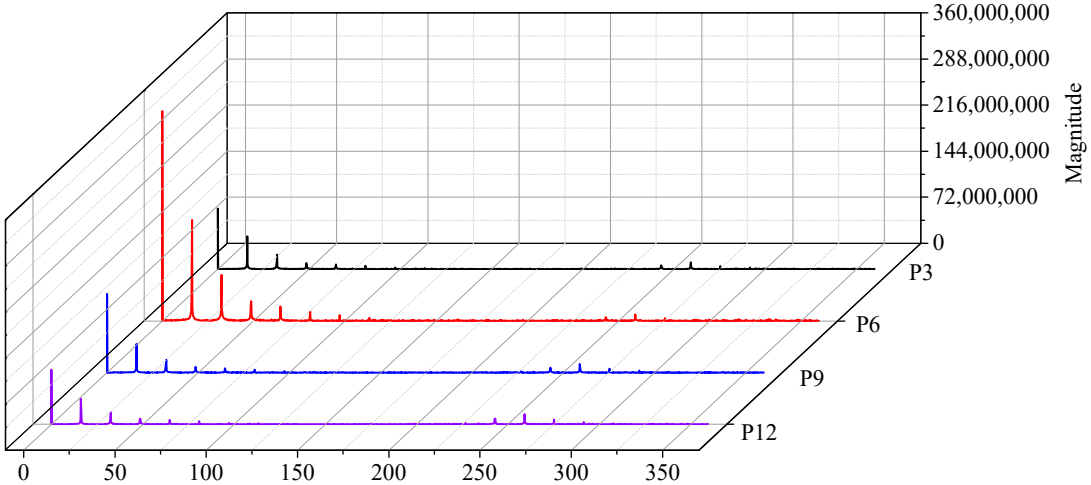

Figure 10. Pressure pulsations at different positions on the tunnel surface.

The results shown in Figure 9 indicate that the peak pressure distribution at different positions changes greatly. Among them, the peak pressure at P5 is the highest, which is about three times that at P11. The peak pressure distribution also coincides with the maximum pressure difference on the blade. Figure 10 shows the pressure pulsations at several key positions during one rotation. It can be concluded that the low-frequency vibration is the strongest, and the flow field in the tunnel changes periodically during the bow thruster's operation.

Based on the pressure variations in the blade and the flow field in the inhomogeneous flow field, the hydrodynamic performance of the bow thruster under different ship advance speeds will be analyzed in detail.

4.2. Hydrodynamic Coefficient Analysis of Bow Thruster in Berthing Direction

The hydrodynamic performance of the bow thruster in the berthing direction is numerically analyzed. The propeller rotation speed remains unchanged at 243 rpm, and the ship advance speeds are 0~3 knots (the speed interval is 1 knot). The propeller's hydrodynamic forces are recorded in the calculation process, and then they are converted into hydrodynamic coefficients. The hydrodynamic coefficients in one cycle at different speeds are shown in Figures 11 and 12, and the time mean results in one cycle are given in Table 3.

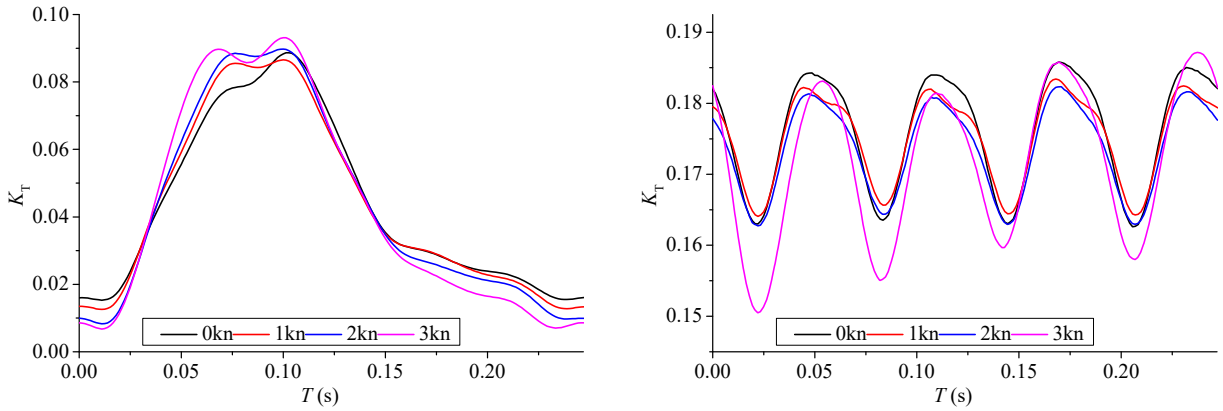

(1) One blade (2) Entire propeller

Figure 11. Thrust coefficient curves in berthing direction.

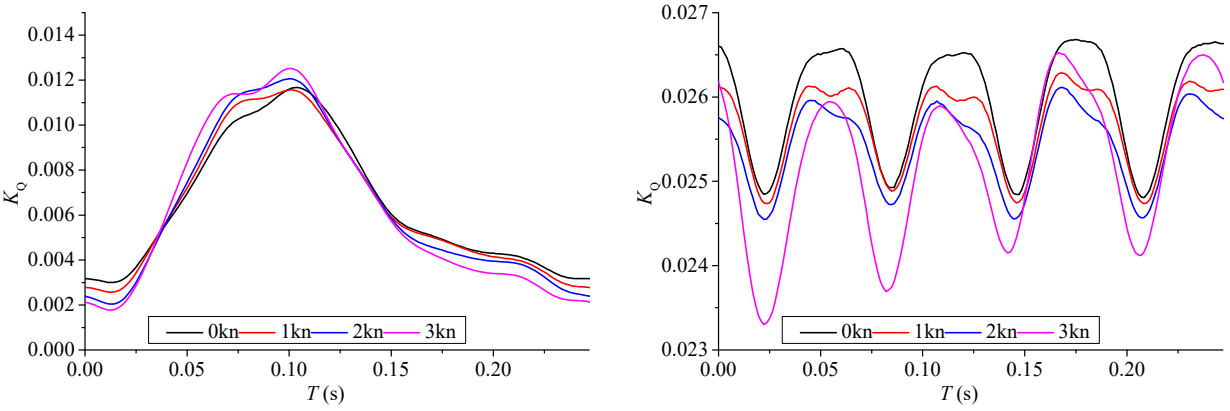

(1) One blade (2) Entire propeller

Figure 12. Torque coefficient curves in berthing direction.

Table 3. Time mean hydrodynamic coefficients of bow thruster in berthing direction.

Advance Speed	K_T (One Blade)	K_T (Entire Propeller)	K_Q (One Blade)	K_Q (Entire Propeller)
0	0.0435	0.176	0.00643	0.0260
1	0.0432	0.175	0.00634	0.0257
2	0.0427	0.173	0.00628	0.0254
3	0.0423	0.171	0.00622	0.0252

By comparing the hydrodynamic coefficient variations, it is found that the thrust coefficient and torque coefficients of the bow thruster decrease gradually with the increase in the ship speed. When the ship speed is increased to 3 knots, the thrusts of one blade and the entire propeller decrease by 2.76% and 2.69%, respectively, and the torques decrease by 3.38% and 3.08%, respectively. At the same time, during the rotation period, the force change amplitude of one blade gradually increases; that is, the vibration of the blade in one cycle is intensified. In addition, the entire propeller force results show that the overall variation amplitude changes slightly when the ship speed is less than 2 knots. Then, the variation amplitude increases when the ship speed is 3 knots. Based on the above results, it can be concluded that the increase in ship speed is unfavorable for the bow thruster's operation.

4.3. Flow Field Distributions in Key Plane of Bow Thruster in Berthing Direction

In order to analyze the hydrodynamic change mechanism of the bow thruster at different ship speeds, the velocity distribution and pressure distribution in the plane where the propeller shaft is located (water depth is 8.6 m) are analyzed. The flow field of the bow thruster is shown in Figures 13 and 14.

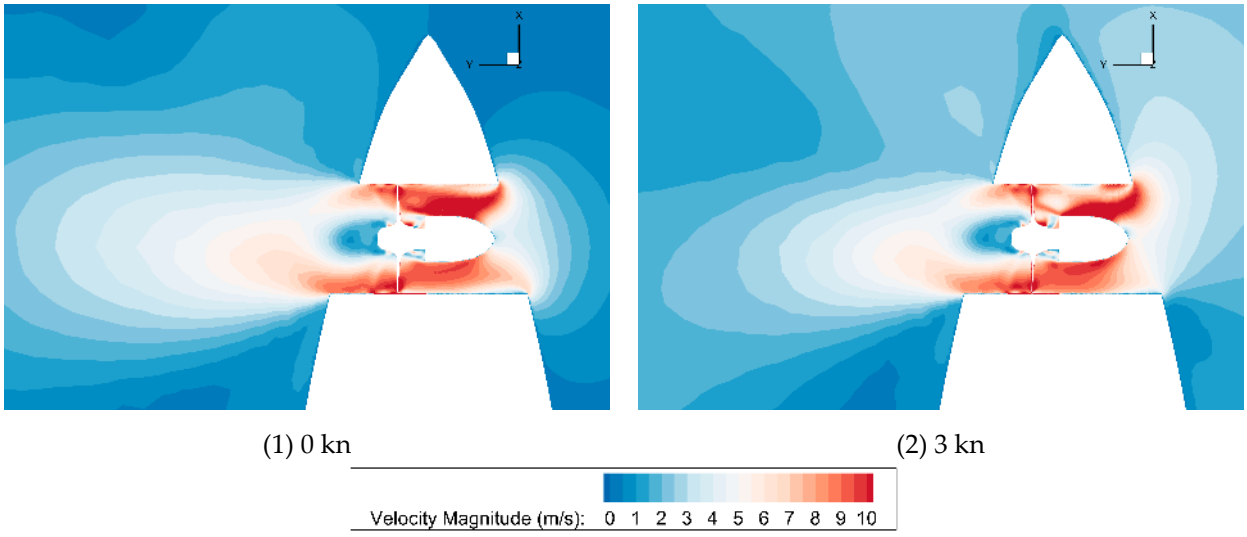

Figure 13. Velocity distributions at propeller shaft depth in berthing direction.

The velocity distributions in the bow thruster tunnel reveal that the tunnel shape is not symmetrical along the propeller axis. The distance between two openings in the bow direction is shorter, where the flow velocity is faster. By contrast, the distance on the other side is longer, and the flow velocity is slower. Accordingly, the flow in the tunnel is asymmetrical when the ship speed is 0 knots. When the ship speed gradually increases, the flow velocity in the negative X-axis direction also increases. The low-speed zone area expands near the inner wall of the tunnel in the bow direction. The flow field change leads to the inflow distribution unevenness and vibration intensification of the propeller. According to the momentum theorem, the greater the velocity differences before and after the propeller become, the greater load the blades bear. As the ship speed increases from

0 to 3 knots, the propeller wake velocity gradually decreases, which results in a gradual decrease in the propeller thrust and torque.

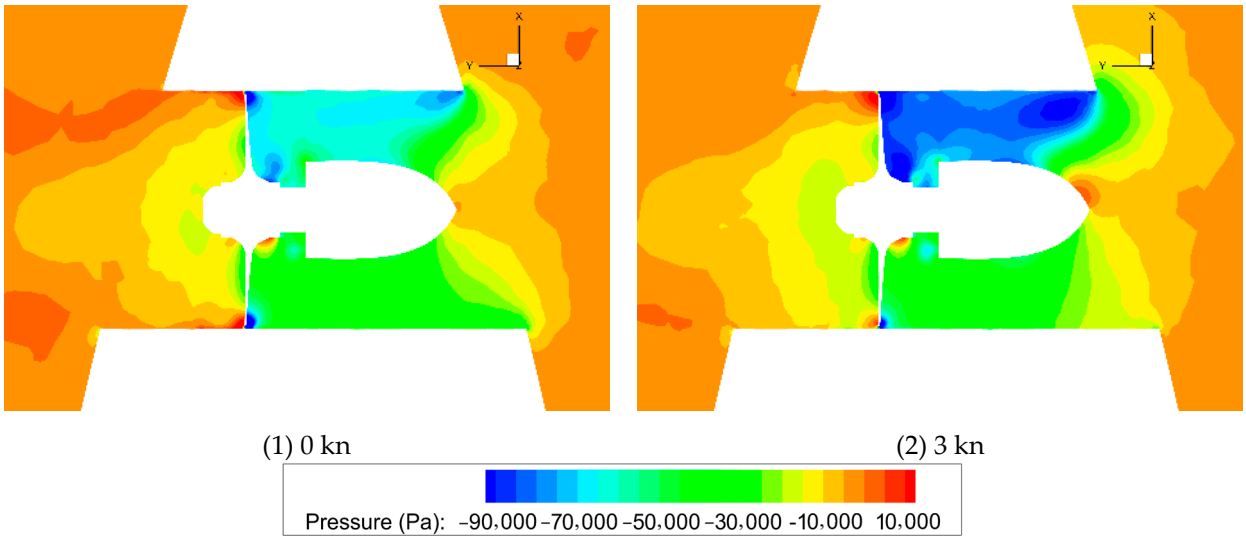

Figure 14. Pressure distributions at propeller shaft depth in berthing direction.

The pressure distributions in the tunnel indicate that the pressure is lower before the propeller and higher after the propeller. Compared with the outlet pressure distribution, the inlet pressure distribution is more uneven, which is affected by the tunnel shape and results in the blade pressure differences at different phases. With the ship speed increase, the outlet pressure changes slightly. In contrast, the inlet pressure changes more obviously. The velocity and pressure changes in the tunnel result in a much larger amplitude of unsteady force on the bow thruster than that of the conventional propeller. Additionally, the faster the ship sails, the greater the amplitude of the blade's vibration.

4.4. Hydrodynamic Coefficient Analysis of Bow Thruster in Departure Direction

In order to compare the hydrodynamic performance of the bow thruster in two directions, the blade pitch in departure direction is adjusted to the same pitch in the berthing direction. Similarly, the propeller rotation speed remains unchanged at 243 rpm, and the ship advance speeds are 0~3 knots (the speed interval is 1 knot). The propeller's hydrodynamic forces are recorded and converted into hydrodynamic coefficients. The hydrodynamic coefficients in one cycle at different speeds are shown in Figures 15 and 16, and the time mean results in one cycle are given in Table 4.

Table 4. Time mean hydrodynamic coefficients of bow thruster in departure direction.

Advance Speed	K_T (One Blade)	K_T (Entire Propeller)	K_Q (One Blade)	K_Q (Entire Propeller)
0	0.0421	0.172	0.00630	0.0256
1	0.0411	0.168	0.00628	0.0255
2	0.0409	0.166	0.00622	0.0252
3	0.0400	0.165	0.00612	0.0250

By comparing the hydrodynamic coefficient variations, the results show that the coefficient variation pattern is similar to that in the berthing direction. When the ship speed is increased to 3 knots, the thrusts of one blade and the entire propeller decrease by 4.99% and 4.07%, respectively, and the torques decrease by 2.86% and 2.34%, respectively. Compared with the conditions in the berthing direction, the inflow change results in a load reduction in the bow thruster, whose thrust decreases by 2.34~4.16%. Meanwhile, the

torque only decreases by less than 1%, which is almost unchanged. It can be observed that the propulsive efficiency becomes worse when leaving port. It is also worth noting that the unsteady force change amplitude of one blade and the entire blade decreases in the departure direction.

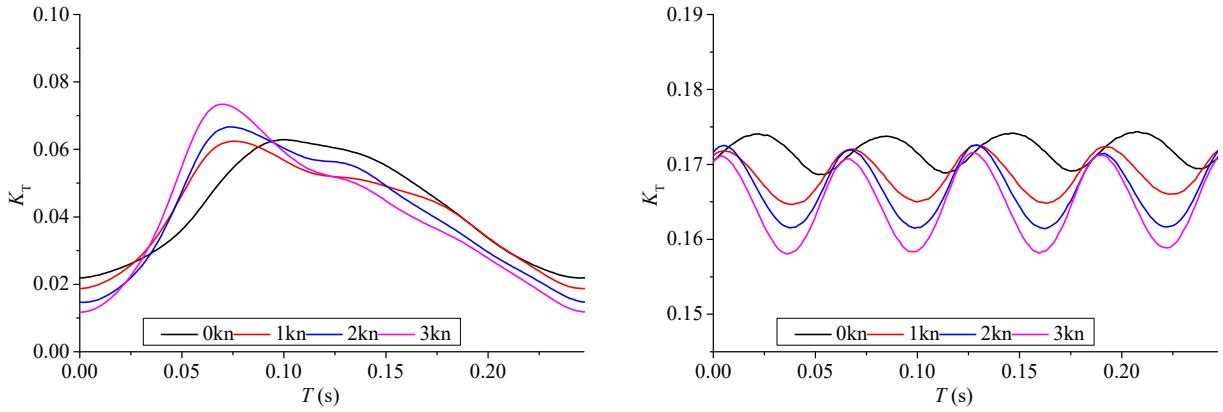

(1) One blade (2) Entire propeller

Figure 15. Thrust coefficient curves in departure direction.

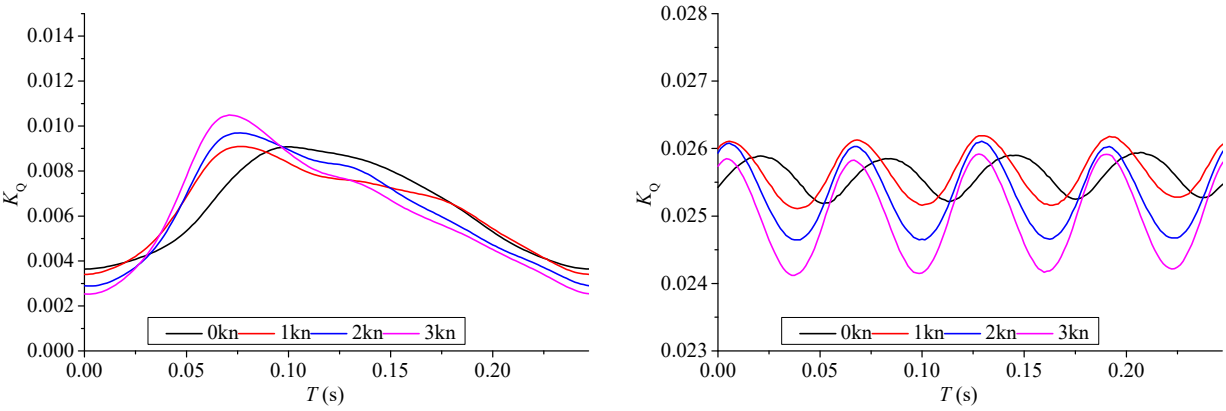

(1) One blade (2) Entire propeller

Figure 16. Torque coefficient curves in departure direction.

4.5. Flow Field Distributions in Key Plane of Bow Thruster in Departure Direction

The velocity distribution and pressure distribution in the plane where the propeller shaft is located (water depth is 8.6 m) are analyzed. The flow field of the bow thruster is shown in Figures 17 and 18.

The velocity distributions in the tunnel reveal that the flow field is not symmetrical, which is similar to the flow field in the berthing direction. As the ship speed increases from 0 to 3 knots, the propeller wake becomes slower. Accordingly, the propeller thrust and torque decrease gradually. In addition, in the departure direction, the blades are closer to the entrance, and there is nothing blocking the inflow. Therefore, the inflow is more uniform, and the unsteady force change amplitude of the propeller is smaller than that in the berthing direction.

The pressure distributions in the tunnel indicate that the pressure distribution is similar to that in the berthing direction. When the ship accelerates, the inflow nonuniformity increases, which leads to a gradual increase in the hydrodynamic difference at different phases of the propeller. Compared with the pressure distributions during berthing, the

pressure distributions before and after the propeller are more uniform, which is consistent with the results of hydrodynamic changes and velocity distributions.

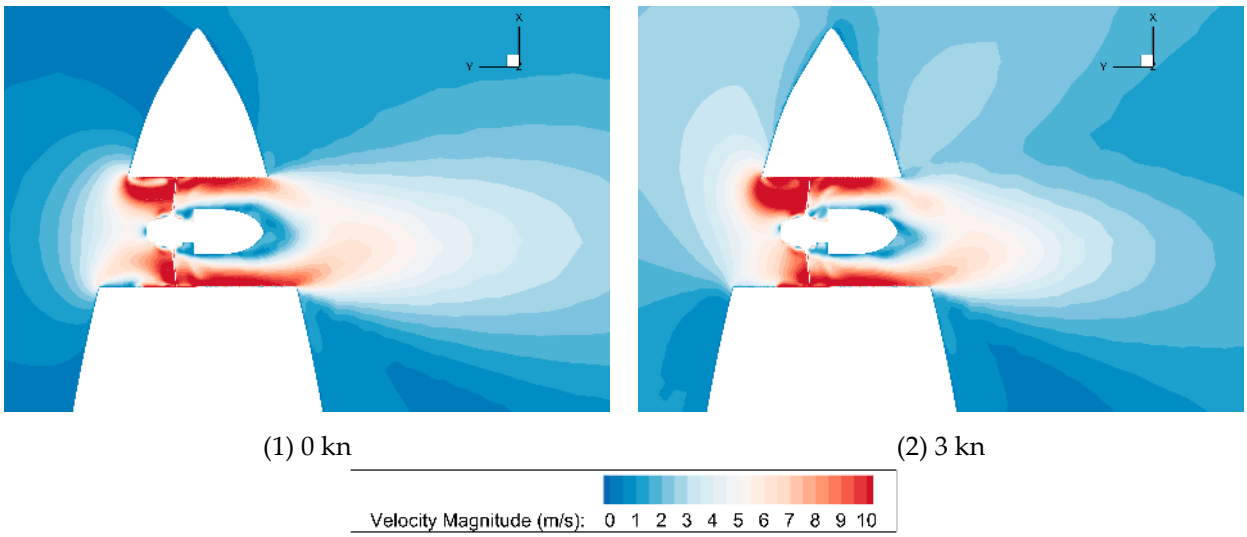

Figure 17. Velocity distributions at propeller shaft depth in departure direction.

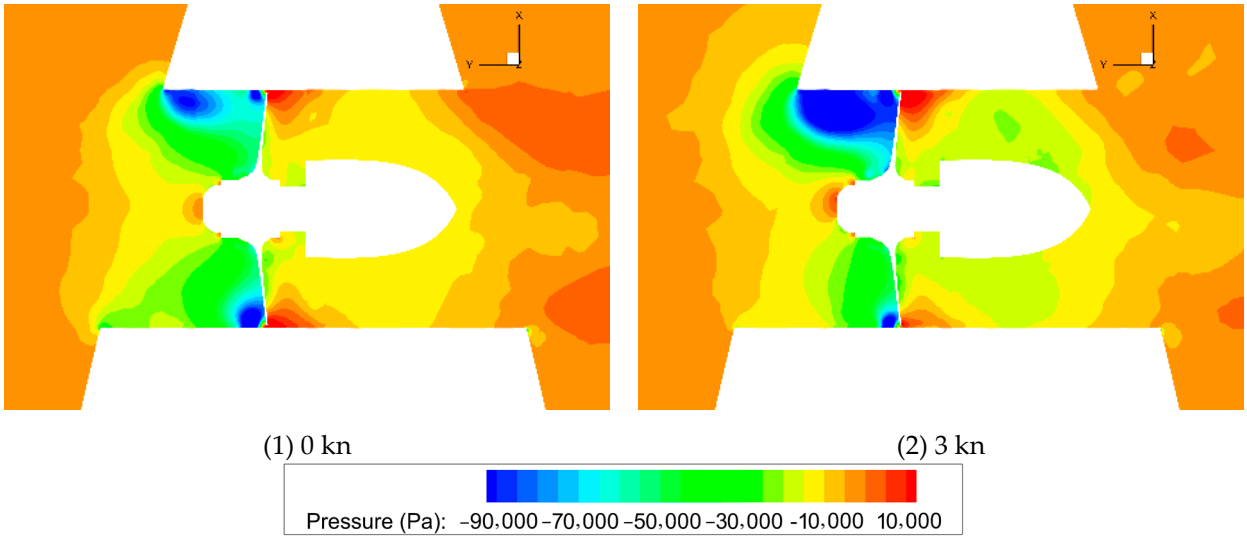

Figure 18. Pressure distributions at propeller shaft depth in departure direction.

According to the hydrodynamic performance variations in pump-jet propulsors in oblique flow [27,28], transverse flow makes the internal flow field of the duct more uneven. The uneven inflow leads to the strengthening of rotor blade vibration and a reduction in propulsive efficiency. We adopted a similar method, and the research conclusion of this paper is basically consistent with the literature's conclusion. Therefore, the research results have certain engineering reference value.

5. Conclusions

Usually, the influence of ship speed on the hydrodynamic performance of bow thrusters was not taken into account in previous related studies. However, during departure and berthing, ships navigate at low speeds, which may change the operation conditions of bow thrusters. Therefore, it is necessary to analyze the impact of changing flow fields on ship maneuvering. Based on the simulation results of this paper, the following conclusions are drawn.

(1) The pressure distribution and peak pressure of the bow thruster at different phases change greatly. The highest peak pressure is about three times the lowest peak pressure. Therefore, the hydrodynamic of the propeller in the tunnel changes periodically during the bow thruster's operation.
(2) With the ship speed increasing to 3 knots, the thrust coefficient and torque coefficient of the bow thruster decrease by 2.69~4.07% and 2.34~3.08%. At the same time, the vibration of one blade and the entire propeller in one cycle is intensified.
(3) Due to the asymmetrical tunnel, the flow velocity is faster in the bow direction and slower in the other direction. Accordingly, the flow in the tunnel is asymmetrical. When the ship speed gradually increases, the low-speed zone area expands near the inner wall of the tunnel in the bow direction, and the propeller wake velocity gradually decreases.
(4) Compared with the outlet pressure distribution, the inlet pressure distribution is more uneven, which results in blade pressure differences at different phases. With the ship speed increase, the outlet pressure changes slightly. In contrast, the inlet pressure changes more obviously.
(5) The coefficient variation patterns are the same in the berthing and departure directions. Meanwhile, in the departure direction, the propeller load is more susceptible to being influenced and decreased by an additional 2.34~4.16% compared with that in the berthing direction. In addition, the unsteady force change amplitude of one blade and the entire blade is smaller in the departure direction.
(6) In the departure direction, the blades are closer to the entrance, and there is nothing blocking the inflow. Therefore, the inflow is more uniform, and the pressure distributions before and after the propeller are more uniform, which is consistent with the results of hydrodynamic changes.

The research work of this paper has a certain reference significance for understanding the hydrodynamic performance of bow thruster operation. However, there is a lack of experimental verification, and relevant experimental plans will be designed for validation in the future.

Author Contributions: Software, Y.S.; validation, T.W.; formal analysis, Y.S.; data curation, X.M. and Y.S.; writing—original draft preparation, H.C. and Y.S.; writing—review and editing, Y.S., Z.Y., Y.T., and J.Z. All authors have read and agreed to the published version of the manuscript.

Funding: This research was funded by NATIONAL NATURAL SCIENCE FOUNDATION OF CHINA, grant number 52371069.

Institutional Review Board Statement: Not applicable.

Informed Consent Statement: Not applicable.

Data Availability Statement: The original contributions presented in the study are included in this article; further inquiries can be directed to the corresponding author.

Conflicts of Interest: The authors declare no conflict of interest.

References

1. Fischer, R. Bow thruster induced noise and vibration. In Proceedings of the Dynamic Positioning Conference, Houston, TX, USA, 17–18 October 2000.
2. Herdzik, J. Proposals and possibilities of unconventional thrusters applications for ship propulsion. *J. KONES* **2009**, *16*, 155–162.
3. Wilkins, J.R. Propeller Design Optimization for Tunnel Bow Thrusters in the Bollard Pull Condition. Doctoral Dissertation, Massachusetts Institute of Technology, Cambridge, MA, USA, 2012.
4. Yao, Z.Q.; Yan, Z.G. Hydrodynamic performance analysis and verification of transverse thrusters. *J. Ship Mech.* **2012**, *16*, 236–245.
5. Terry, S. A Study of the Hydrodynamic Interactions Between Bow Thrusters. *Catal. Sci. Technol.* **2015**, *6*, 677–680.
6. Wang, H.L.; Lin, J.; Cao, L.Q.; Lv, W.F.; Wang, C.; Lu, G.X. Research on the Bow Thruster of Large Ship. In Proceedings of the 2015 4th International Conference on Mechatronics, Materials, Chemistry and Computer Engineering, Atlantis, Xi'an, China, 12–13 January 2015.
7. Theophilus-Johnson, K. Design analysis of fast crew vessel bow thrusters. *J. Oil Gas Technol.* **2017**, *08*, 1955–1962.

8. Feng, Y.K.; Chen, Z.G.; Dai, Y.; Cui, L.Z.; Zhang, Z.; Wang, P. An experimental and numerical investigation on hydrodynamic characteristics of the bow thruster. *Ocean Eng.* **2020**, *209*, 107348.
9. Teresa, A.G.; Miroslaw, K.G. Experimental study on the selected aspects of bow thruster generated flow field at ship zero-speed conditions. *Ocean Eng.* **2020**, *209*, 107463.
10. Feng, Y.K.; Chen, Z.G.; Dai, Y.; Cui, L.Z.; Zhang, Z.; Wang, P. Multi-objective optimization of a bow thruster based on URANS numerical simulations. *Ocean Eng.* **2022**, *247*, 110784. [CrossRef]
11. Bui, T.D. Numerical simulation of the performance of bow thruster taking into account turbulence model influence using RANS method. In Proceedings of the 7th International Symposium on Marine Propulsors, Wuxi, China, 17–21 October 2022.
12. Huang, W.C.; He, W.; Li, Z.R. Hydrodynamic performance prediction of a tunnel thruster under berthing and unberthing conditions. In Proceedings of the International Ocean and Polar Engineering Conference, Ottawa, ON, Canada, 19–23 June 2023.
13. Kazemi, M.; Kornev, N.; Hinnenthal, J. Scale resolving simulation of unsteady bow thruster hydrodynamics. *Ocean Eng.* **2024**, *298*, 117212. [CrossRef]
14. Li, D.Q. Validation of RANS predictions of open water performance of a highly skewed propeller with experiments. *J. Hydrodyn. Ser. B* **2006**, *18*, 520–528. [CrossRef]
15. Song, B.W.; Wang, Y.J.; Tian, W.L. Open water performance comparison between hub-type and hubless rim driven thrusters based on CFD method. *Ocean Eng.* **2015**, *103*, 55–63. [CrossRef]
16. Tu, T.N. Numerical simulation of propeller open water characteristics using RANSE method. *Alex. Eng. J.* **2019**, *58*, 531–537. [CrossRef]
17. Guo, H.P.; Zou, Z.J.; Wang, F.; Liu, Y. Numerical investigation on the hydrodynamic characteristics of a marine propeller operating in oblique inflow. *Appl. Ocean Res.* **2019**, *93*, 101969. [CrossRef]
18. Lee, H.M.; Lu, Z.B.; Lim, K.M.; Xie, J.L.; Lee, H.P. Quieter propeller with serrated trailing edge. *Appl. Acoust.* **2019**, *146*, 227–236. [CrossRef]
19. Huang, X.C.; Shi, S.K.; Su, Z.W.; Tang, W.H.; Hua, H.X. Reducing underwater radiated noise of a SUBOFF model propelled by a pump-jet without tip clearance: Numerical simulation. *Ocean Eng.* **2022**, *243*, 110277. [CrossRef]
20. Qin, D.H.; Pan, G.; Lee, S.; Huang, Q.G.; Shi, Y. Underwater radiated noise reduction technology using sawtooth duct for pumpjet propulsor. *Ocean Eng.* **2019**, *188*, 106228. [CrossRef]
21. Sun, Y.; Liu, W.; Li, T.Y. Numerical investigation on noise reduction mechanism of serrated trailing edge installed on a pump-jet duct. *Ocean Eng.* **2019**, *191*, 106489. [CrossRef]
22. Sun, Y.; Qu, L.X.; Peng, H.H.; Guo, J.M.; Xiong, Z.X. Numerical simulation of hydrodynamic performance of pump-jet propulsor with serrated trailing-edge duct under different working conditions. *Ocean Eng.* **2023**, *290*, 116323. [CrossRef]
23. Versteeg, H.K.; Malalasekera, M. *An Introduction to Computational Fluid Dynamics: The Finite Volume Method*; Springer: Berlin/Heidelberg, Germany, 1990; Volume I and II.
24. Menter, F.R. Two-equation eddy-viscosity turbulence models for engineering applications. *AIAA J.* **1994**, *32*, 1598–1605. [CrossRef]
25. Tu, Y.J.; Yeoh, G.H.; Liu, C. Computational Fluid Dynamics: A Practical Approach. *Artif. Organs* **2012**, *33*, 727–732.
26. Ding, Y.L.; Song, B.W.; Wang, P. Numerical investigation of tip clearance effects on the performance of ducted propeller. *Ocean Eng.* **2015**, *7*, 795–804.
27. Qiu, C.; Huang, Q.; Pan, G.; Shi, Y.; Dong, X.G. Numerical simulation of hydrodynamic and cavitation performance of pumpjet propulsor with different tip clearances in oblique flow. *Ocean Eng.* **2020**, *209*, 107285. [CrossRef]
28. Peng, H.; Guo, J.M.; Sun, Y.; Wang, G.; Qu, L.X. Numerical analysis of hydrodynamic force of front- and rear-stator pump-jet propulsion systems behind a submarine under oblique sailing. *Ocean Eng.* **2022**, *266*, 112565. [CrossRef]